

pubs.acs.org/NanoLett Letter

Hysteretic Magnetoresistance in a Non-Magnetic SrSnO₃ Film via Thermal Coupling to Dynamic Substrate Behavior

Laxman Raju Thoutam,* Tristan K. Truttmann, Anil Kumar Rajapitamahuni, and Bharat Jalan*



Cite This: Nano Lett. 2021, 21, 10006-10011



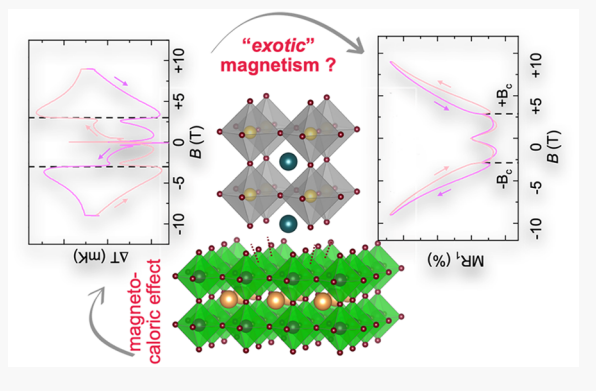
ACCESS

Metrics & More

Article Recommendations

Supporting Information

ABSTRACT: Hysteretic magnetoresistance (MR) is often used as a signature of ferromagnetism in conducting oxide films and heterostructures. Here, magnetotransport is investigated in a nonmagnetic Ladoped SrSnO₃ film. A 12 nm La:SrSnO₃/2 nm SrSnO₃/GdScO₃ (110) film with insulating behavior exhibited a robust hysteresis loop in the MR at T < 5 K accompanied by an anomaly at $\sim \pm 3$ T at T < 2.5 K. Furthermore, MR with the field in-plane yielded a value exceeding 100% at 1.8 K. Using detailed temperature-, angle- and magnetic field-dependent resistance measurements, we illustrate the origin of hysteresis is not due to magnetism in the film but rather is associated with the magnetocaloric effect of the substrate. Given GdScO₃ and similar substrates are commonly used, this work highlights the importance of thermal coupling to processes in the substrates which must be carefully



accounted for in the data interpretation for heterostructures utilizing these substrates.

KEYWORDS: complex oxides, hysteresis, magnetoresistance, ferromagnetism, magnetocaloric effect, alkaline-earth stannates

■ INTRODUCTION

The choice of substrate has a dramatic effect on complex oxide film properties. Most obviously, the use of a chemically compatible and lattice-matched substrate promotes high structural quality of the grown film. The complex oxide thin film community has also discovered more nuanced effects from the substrate including the ability to strain engineer films, 1-4 confer its octahedral rotations to the films, 5-7 and to use an intrinsic electric field to electrostatically dope the film.⁸⁻¹¹ However, these effects are all static in the sense that the substrate is bestowing properties to the film through a fixed structural or physical relationship; there has been very little attention paid to how dynamic behavior in the substrate might influence the film. For instance, if a substrate exhibits the magnetocaloric effect (i.e., the generation or consumption of heat due to a change in applied magnetic field), it can potentially have a tremendous impact on the magnetotransport behavior of the films. 12 Therefore, it can also hinder our ability to interpret data and may even lead to misinterpretation.

To study this effect, we use $SrSnO_3$ (SSO) thin films. This material belongs to a family of nonmagnetic alkaline-earth stannates ($ASnO_3$; A = Ca, Sr or Ba), which have gained significant interest in recent years owing, in large part, to their (ultra)wide bandgap and high room-temperature electron mobility. These characteristics of stannates have paved the way for their use in transparent and high-power electronic applications. Motivated by this, significant progress has been made in synthesizing $BaSnO_3$ (BSO) and SSO films with

atomic layer control using a variety of growth methods. ^{15–21} Although there are no studies of transport in bulk SSO single crystals, several exciting developments have occurred in SSO thin films including the demonstration of oxygen vacancy-induced room-temperature ferromagnetism, ^{22,23} high conductivity, ²⁴ a weak localization and Aronov–Altshuler electron–electron interaction, ²⁵ a large phase coherence length, ²⁵ and several field-effect devices ^{26–28} including those operating at GHz frequencies. ²⁹ As we will show, the insulating transport behavior achievable in this material make it a highly sensitive probe for the subtle thermal effects arising from the substrate. We therefore choose this material as a case study in thermal coupling between a film and processes that occur in the substrate. We note that our observation is applicable to any other films and heterostructures on these substrates with resistivity that is a strong function of temperature.

Using 12 nm La-doped SSO films grown on a 2 nm insulating SSO buffer layer on a GdScO₃ (GSO) (110) substrate, we discovered a large magnetoresistance (MR) at 1.8 K exceeding 100% accompanied by a hysteretic behavior. While this may *appear* to be indicative of exotic magnetism in

Received: September 21, 2021
Revised: November 10, 2021
Published: November 22, 2021





Nano Letters pubs.acs.org/NanoLett Letter

otherwise nonmagnetic SSO films, we show otherwise. Rather, it is due to thermal coupling between the film and the magnetocaloric behavior of the GSO substrate. We provide critical insight into the role of substrates on the magnetotransport measurements of films despite them being insulating.

The SSO/GSO film used in this study was grown using hybrid MBE. ^{30,31} Figure 1(a) shows a high-resolution on-axis

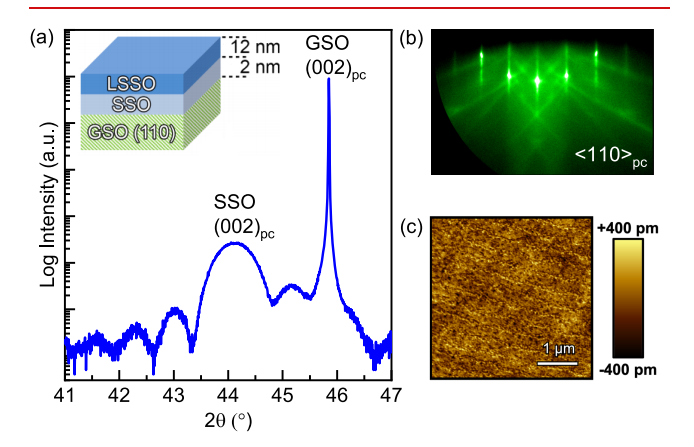


Figure 1. (a) High-resolution X-ray $2\theta-\omega$ coupled scan of a 12 nm La:SSO/2 nm SSO/GSO (110). The subscript pc denotes pseudocubic notation. The schematic of the structure is shown in the inset. (b) RHEED pattern along the substrate edge and (c) atomic force microscopy of the sample, showing a smooth surface morphology.

wide-angle X-ray diffraction $2\theta-\omega$ scan of a 12 nm La:SSO/2 nm SSO/GSO (110) revealing an expanded out-of-plane lattice parameter of 4.102 \pm 0.002 Å. This value is consistent with the coherently strained tetragonal SSO phase on the GSO substrate. The SSO film is thus phase-pure, epitaxial, and fully strained on the GSO (110) substrate. Finite-thickness fringes were also observed, indicating laterally homogeneous films and an abrupt smooth interface. The streaky reflection high-energy electron diffraction (RHEED) pattern (Figure 1(b)) and atomic force microscopy (AFM) images (Figure 1(c)) confirm atomically smooth surfaces.

Figure 2 shows the magnetotransport results from this sample showing temperature-dependent sheet resistance (R_s) and MR. The room-temperature Hall-effect measurements yielded a carrier concentration of $1.9 \times 10^{19} \text{ cm}^{-3}$ in this sample. Figure 2(a) shows an insulating-like behavior, i.e., an increasing sheet resistance with decreasing temperature, which we attribute to the disorder at the surface. 32 A sharp rise in R_s was observed at T < 6 K. To investigate the low-temperature transport mechanism, we performed Zabrodski analysis (see inset of Figure 2(a)), yielding a slope of 0.6. This result reveals that the low-temperature (T < 6 K) insulating behavior is associated with the Efros-Shklovskii (ES) variable range hopping. The exponential temperature dependence from this mechanism will be important for its strong response to small temperature changes. We also measured the MR, defined as $100\% \times [R(\mathbf{B}) - R(0)]/R(0)$, where $R(\mathbf{B})$ is the sheet resistance at a magnetic-field, B. The MR with the field out of plane was measured at different temperatures by sweeping B from $0 \text{ T} \rightarrow 9 \text{ T} \rightarrow -9 \text{ T} \rightarrow 0 \text{ T}$ at 100 Oe/s. Figure 2 panels (b) and (c) show MR as a function of **B** at 6 K \leq $T \leq$ 200 and 1.8 K $\leq T \leq$ 5 K, respectively. The evolution of MR as a function of temperature at B = 9 T is shown in Figure 2(d). Several observations can be made here. First, with decreasing

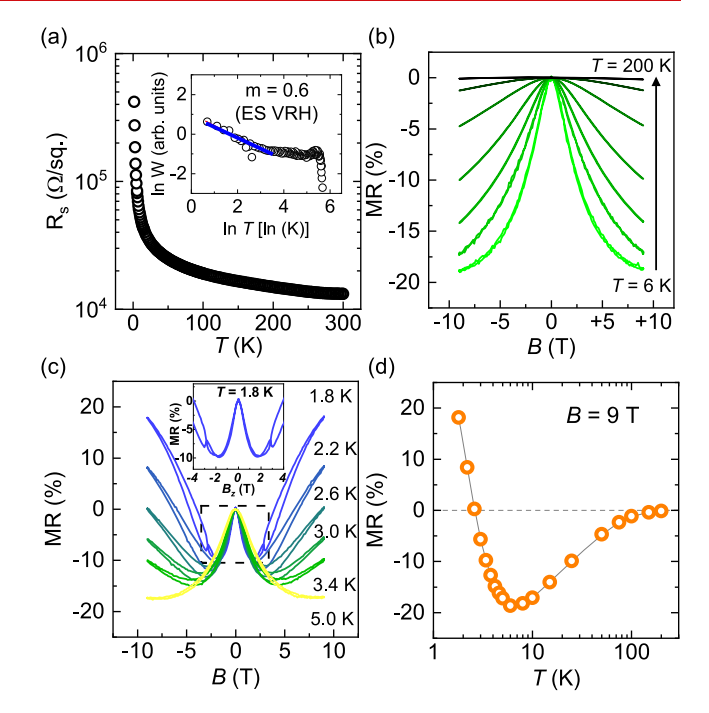


Figure 2. (a) Temperature-dependent sheet resistance (R_s) of 12 nm La:SSO/2 nm SSO/GSO (110). The inset shows ln W vs ln T (Zabrodski plot) where $W=-\mathrm{d}\ln(\rho)/\mathrm{d}\ln(T)$, yielding an exponent m in $\rho=\rho_0\exp(T_0/T)^m$ as the slope. The value of m close to 0.5 is consistent with Efros–Shklovskii variable range hopping. (b) Perpendicular MR at various constant temperatures from $6~\mathrm{K} \leq T \leq 200~\mathrm{K}$. (c) Low-temperature ($T \leq 5~\mathrm{K}$) perpendicular MR shows a crossover from negative to positive magnetoresistance with applied field. Inset shows the zoom-in figure revealing an anomaly (sudden drop in resistance) and the hysteresis in MR. (d) MR as a function of temperature for $B=9~\mathrm{T}$.

T, a crossover from a negative MR (6 K \leq T \leq 200 K) to a combination of a negative and positive MR (1.8 K \leq T \leq 5 K) occurs. Second, the magnetic field at which a crossover from negative to positive MR occurs decreases with decreasing temperature. Third, a surprising but robust hysteresis behavior appears at 1.8 K \leq T \leq 5 K accompanied by an anomaly around \pm 3 T at T \leq 2.4 K (see inset of Figure 2(c)). We first discuss the origin of a negative and a positive MR and then return to the discussion of a rather unusual hysteresis behavior.

The presence of negative and positive MR in the hopping regime is seen previously in other semiconducting materials including n-type CuGaSe₂,³³ GaAs,^{34,35} and most recently stannates.^{36,37} The negative MR at low field can be understood in terms of suppression of the destructive interference between forward scattering paths of the hopping electron for a given initial and final state of hop.^{35,37} Likewise, the positive MR can be explained by the shrinkage of the localized wave function of the electrons in the presence of applied magnetic field, resulting in the reduction of the overlap between neighboring hopping sites, causing an increase of resistance with increasing field.³⁸ The fact that the field at which crossover takes place decreases with decreasing temperature is again consistent with a crossover from a weak localization at higher temperatures to strongly localized transport at low temperatures.

To get further insights into the observed MR behavior, we performed angle-dependent MR measurements at 1.8 K using two different current directions $(I_y \text{ vs } I_x)$ as illustrated in the inset of Figure 3(a),(b). We define the MR from these two

Nano Letters pubs.acs.org/NanoLett Letter

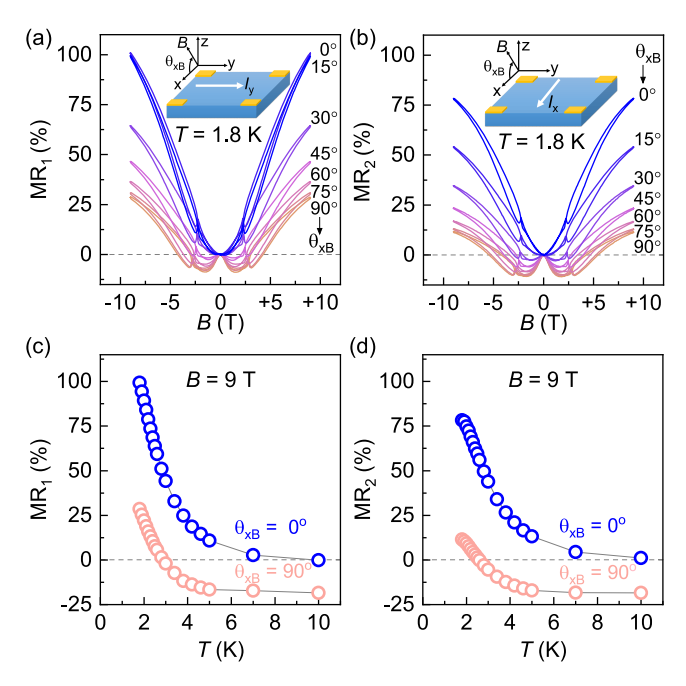


Figure 3. Angle-dependent MR at T=1.8 K for two different configurations with (a) $I\perp x$ and (b) $I\parallel x$. Insets show the measurement configuration. **B** is out-of-plane to the sample surface when $\theta_{xB}=0^{\circ}$ and in-plane when $\theta_{xB}=90^{\circ}$. (c, d) Temperature-dependent anisotropic MR at **B** = 9 T in each configuration for $\theta_{xB}=0^{\circ}$ and $\theta_{xB}=90^{\circ}$.

configurations as MR₁ and MR₂. Regardless of the current directions $(I_y \text{ vs } I_x)$, both MR₁ and MR₂ revealed the suppression of low-field negative MR as field sweeps from the out-of-plane ($\theta_{xB} = 90^{\circ}$) to the in-plane ($\theta_{xB} = 0^{\circ}$) direction. This observation is again consistent with the previous reports $(In_2O_{3-\omega}^{39,40})$ n-type GaAs³⁴) of the angledependent anisotropic behavior in the strong localization regime. These results further revealed a strong anisotropy in the MR, specifically, in the high-field regime, as a function of θ_{xB} . MR₁ and MR₂ reach ~100% and ~75% at 1.8 K, respectively, when θ_{xB} reaches 0° , i.e., magnetic-field in the plane of the sample. The small difference in the values of the MR₁ and MR₂ is likely due to different starting values of the resistance, i.e., $(R_1(0) > R_2(0))$ in these two configurations. A slight difference in the resistance value is likely due to crystallographic anisotropy of the GSO (110) substrate. The observed high value of in-plane MR is again consistent with transport in the strong localization regime where the application of magnetic-field is expected to distort the electron wave function impacting the overlap between the hopping sites and consequently the MR.³⁸ A similar behavior was observed previously in GaAs in the strong localization regime. 41,42 We further show in Figure 3(c),(d) MR₁ and MR₂ measured at θ_{xB} = 90° and 0° as a function of temperature. Consistent with the onset of strong localization at \tilde{T} < 6 K, these results again revealed an increase in MR below ~6 K, suggesting the origin of the large MR is associated with transport in the strong localization regime.

We now return to the discussion of the hysteresis and the anomaly in the MR measurements. For brevity, we only show MR_1 , i.e., when current is along the *y*-direction (see the inset of Figure 3(a)). Before we discuss these data, it is important to show the experimental setup illustrating the sample mount and how sample temperature was recorded. As shown in Figure

4(a), the sample is first glued using electrically insulating varnish from LakeShore Cryotronics onto a sample holder,

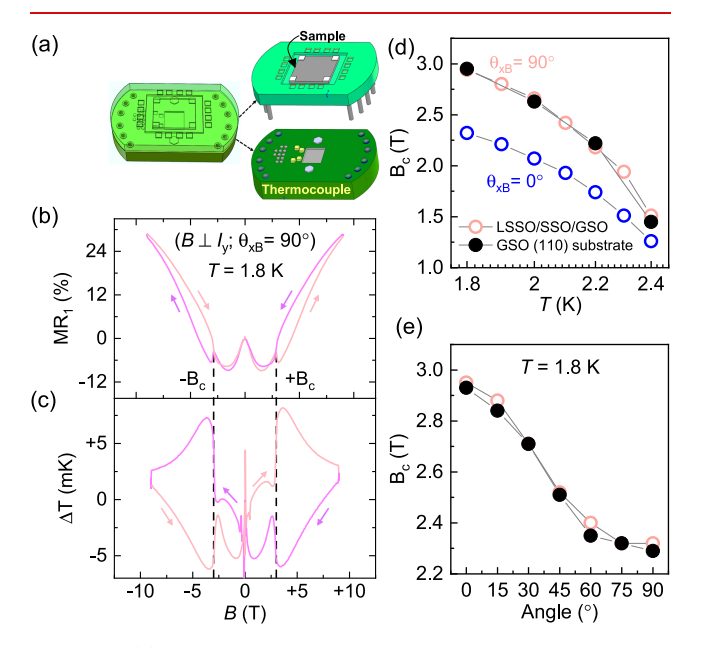


Figure 4. (a) Schematic of the measurement setup illustrating the position of the sample and thermocouple. (b) Hysteretic MR at T=1.8 K for configuration 1 with the field out-of-plane ($\theta_{xB}=90^{\circ}$). \mathbf{B}_{c} represents the critical field at which an anomaly in MR appears. (c) Evolution of the thermocouple temperature of the sample during the field sweep from 0 T \rightarrow 9 T \rightarrow -9 T \rightarrow 0 T. (d) Temperature-dependent \mathbf{B}_{c} for 12 nm La:SSO/2 nm SSO/GSO and a bare GSO substrate for $\theta_{xB}=90^{\circ}$ and 0° . (e) Angle-dependent critical field at T=1.8 K for \mathbf{B}_{c} for a 12 nm La-doped SSO/2 nm undoped SSO/GSO and a bare GSO substrate.

which is then mounted onto the Dynacool rotator puck, which has an on-board thermocouple (shown as yellow dots in Figure 4(a)) that accurately measures the temperature of the sample. Figure 4(b) shows MR₁ at $\theta_{xB} = 90^{\circ}$ and T = 1.8 K during the field sweep $0 \text{ T} \rightarrow 9 \text{ T} \rightarrow -9 \text{ T} \rightarrow 0 \text{ T}$ at a rate of 100 Oe/s, revealing a clear hysteresis and an anomaly at ~±3 T (marked as B_c). The anomaly occurs at an identical critical field, B_c during the forward and reverse field sweeps. This can be seen clearly in Figure S1 using the first derivate of the MR₁ with respect to B. Figure 4(c) shows the thermocouple temperature deviation from the set point during the sweep as a function of B. This plot reveals a hysteretic temperature behavior and a sudden change in temperature at Bc, the same critical field where an anomaly in MR was seen. The change in temperature at B_c is ~8 mK. We attribute the hysteretic temperature and the sudden change in temperature at Bc being responsible for the MR hysteresis and the anomaly. Since the low-temperature resistance of the sample is an exponential function of temperature, even small changes in temperature can introduce observable changes in the resistance. However, it raises additional questions: what is the origin of hysteretic temperature, and why there is a sudden change in temperature at B_c?

To investigate these questions, we measured the variation in temperature of a bare GSO (110) substrate without any SSO film in the same way as in Figure 4(c). Surprisingly, the bare substrate yielded an identical hysteretic behavior in temperature as a function of magnetic field accompanied by the same anomaly at \mathbf{B}_c (Figure S2). The bare substrate also showed an anomaly in temperature hysteresis at \mathbf{B}_c , which persisted at T

 \leq 2.4 K. The value of \mathbf{B}_{c} from the temperature hysteresis of the bare GSO substrate, and from the MR hysteresis of the 12 nm La:SSO/2 nm SSO/GSO (110) is depicted in Figure 4(d),(e) as a function of T and angle θ_{xB} , respectively. Open symbols correspond to data from the La:SSO/SSO/GSO whereas the solid symbols represent the bare GSO substrate. An identical value of \mathbf{B}_{c} as a function of T and θ_{xB} was observed between La:SSO/SSO/GSO and the bare substrate. The difference between \mathbf{B}_{c} for the out-of-plane and in-plane directions is likely due to the distorted orthorhombic structure of GSO substrate. A similar magnetic anisotropy with a preferred easy axis and hard axis along different crystallographic directions was seen in a similar rare-earth perovskite scandate substrate DyScO₃. To this end, it becomes apparent that the origin of hysteresis and the anomaly in MR is related to the substrate.

But then why does the anomaly disappear at T > 2.4 K and what is the physical significance of B_c? We explain this due to the antiferromagnetic transition in GSO. GSO has a distorted orthorhombic structure with an antiferromagnetic ordering below the Néel temperature $T_N = \sim 2.6 \text{ K}^{44}$ and is also shown to exhibit reversible magnetocaloric properties. 45 An external magnetic field disfavors the antiferromagnetic state, so below T_N, a magnetic field can induce a phase transition to the paramagnetic state. Thus, the feature associated with the anomaly in the MR at T < 2.4 K can be attributed to the magnetic-field induced phase-transition between GSO's antiferromagnetic at low fields to its paramagnetic state at high fields. In the paramagnetic state, the increasing magnitude of the applied field aligns the spin dipoles to field direction. This spin alignment lowers the entropy of the spin system, which is balanced by releasing heat to the lattice. This behavior raises the sample temperature and consequently lowers the film resistance resulting in the hysteresis above the critical field or for any field for temperatures immediately above $T_{\rm N}$. According to this description, decreasing ramp rates should lower the hysteresis, which we confirmed in Figure S3 and the accompanying discussion.

In summary, using detailed magnetotransport measurements in La-doped SSO films on the GSO substrate, we discuss the origin of a large MR exceeding 100% in an insulating SSO film owing to the transport in the strong localization regime. It was found that this sample also exhibits a robust hysteresis in MR suggesting an apparent emergence of exotic magnetism in an otherwise nonmagnetic La-doped SSO film. However, we provide clear evidence that thermal coupling between the SSO film and the magnetocaloric effect of the GSO substrate is responsible for the hysteresis behavior. We further found an anomaly in MR which was attributed to the field-induced antiferromagnetic → paramagnetic phase transition in GSO substrate below the Néel temperature. Two other commonly used rare-earth scandate substrates TbScO₃ and DyScO₃ have also demonstrated antiferromagnetism with similar Néel temperatures, 43,44,46 and a strong magnetocaloric effect has also been measured for DyScO₃. 47 These findings further suggest that the thermal coupling between films and substrates—especially these rare-earth scandate substrates must be considered in the interpretation of any ostensible magnetism observed in complex oxides heterostructures.

■ EXPERIMENT

The epitaxial La-doped SSO film was grown on GSO (110) substrates using a radical-based molecular beam epitaxy approach. Details of growth conditions can be found

elsewhere. 19,30,31,37 A brief discussion is presented here. Sr and La were evaporated using effusion cells, and oxygen was supplied using a RF plasma source operating at 250 W. Sn is supplied using a metal—organic chemical precursor, hexamethylditin (HMDT). The film was grown at a substrate temperature of 950 °C (thermocouple temperature), and at a fixed oxygen background pressure of 5×10^{-6} Torr. Electronic transport measurements were performed in a Quantum Design Physical Property Measurement System (Quantum Design Dynacool) using a van der Pauw configuration. Indium was used as an ohmic contact.

ASSOCIATED CONTENT

Supporting Information

The Supporting Information is available free of charge at https://pubs.acs.org/doi/10.1021/acs.nanolett.1c03653.

First derivative of MR1 with respect to the applied magnetic field, temperature change of a bare GdScO3 (110) substrate, perpendicular MR, and schematic of the 12 nm LSSO/2 nm SSO/GSO structure (PDF)

AUTHOR INFORMATION

Corresponding Authors

Laxman Raju Thoutam — Department of Chemical
Engineering and Materials Science, University of Minnesota Twin Cities, Minneapolis, Minnesota 55455, United States;
Present Address: Department of Electronics and
Communications Engineering, SR University, Warangal
Urban, Telangana 506371, India; Email: tlaxmanraju@gmail.com

Bharat Jalan – Department of Chemical Engineering and Materials Science, University of Minnesota - Twin Cities, Minneapolis, Minnesota 55455, United States; oorcid.org/0000-0002-7940-0490; Email: bjalan@umn.edu

Authors

Tristan K. Truttmann – Department of Chemical Engineering and Materials Science, University of Minnesota - Twin Cities, Minneapolis, Minnesota 55455, United States

Anil Kumar Rajapitamahuni – Department of Chemical Engineering and Materials Science, University of Minnesota -Twin Cities, Minneapolis, Minnesota 55455, United States

Complete contact information is available at: https://pubs.acs.org/10.1021/acs.nanolett.1c03653

Notes

The authors declare no competing financial interest. The data that support the findings of this study are available from the corresponding author upon reasonable request.

ACKNOWLEDGMENTS

The authors acknowledge Fengdeng Liu for the illustration of the Dynacool rotator puck. This work was supported primarily by the National Science Foundation (NSF) through the University of Minnesota MRSEC under Award Number DMR-2011401. Part of this work was supported through the Air Force Office of Scientific Research (AFOSR) through Grant No. FA9550-19-1-0245 and FA9550-21-1-0025 and through NSF DMR-1741801. Portions of this work were conducted in the Minnesota Nano Center, which is supported by the National Science Foundation (NSF) through the National Nano Coordinated Infrastructure Network (NNCI) under

Award Number ECCS-1542202. Part of this work was also carried out in the College of Science and Engineering Characterization Facility, University of Minnesota, which has received capital equipment funding from the NSF through the UMN MRSEC program.

REFERENCES

- (1) Ahadi, K.; Galletti, L.; Li, Y.; Salmani-Rezaie, S.; Wu, W.; Stemmer, S. Enhancing superconductivity in $SrTiO_3$ films with strain. *Science Advances* **2019**, 5 (4), eaaw0120.
- (2) Hu, S.; Cazorla, C.; Xiang, F.; Ma, H.; Wang, J.; Wang, J.; Wang, X.; Ulrich, C.; Chen, L.; Seidel, J. Strain Control of Giant Magnetic Anisotropy in Metallic Perovskite $SrCoO_{3-\delta}$ Thin Films. ACS Appl. Mater. Interfaces 2018, 10 (26), 22348–22355.
- (3) Schlom, D. G.; Chen, L.-Q.; Eom, C.-B.; Rabe, K. M.; Streiffer, S. K.; Triscone, J.-M. Strain Tuning of Ferroelectric Thin Films. *Annu. Rev. Mater. Res.* **2007**, *37* (1), 589–626.
- (4) Schlom, D. G.; Chen, L.-Q.; Fennie, C. J.; Gopalan, V.; Muller, D. A.; Pan, X.; Ramesh, R.; Uecker, R. Elastic strain engineering of ferroic oxides. *MRS Bull.* **2014**, *39*, 118.
- (5) Rondinelli, J. M.; May, S. J.; Freeland, J. W. Control of octahedral connectivity in perovskite oxide heterostructures: An emerging route to multifunctional materials discovery. *MRS Bull.* **2012**, *37*, 261.
- (6) Liao, Z.; Huijben, M.; Zhong, Z.; Gauquelin, N.; Macke, S.; Green, R. J.; Van Aert, S.; Verbeeck, J.; Van Tendeloo, G.; Held, K.; Sawatzky, G. A.; Koster, G.; Rijnders, G. Controlled lateral anisotropy in correlated Manganite heterostructures by interface-engineered oxygen octahedral coupling. *Nat. Mater.* **2016**, *15*, 425.
- (7) Bousquet, E.; Dawber, M.; Stucki, N.; Lichtensteiger, C.; Hermet, P.; Gariglio, S.; Triscone, J.-M.; Ghosez, P. Improper ferroelectricity in perovskite oxide artificial superlattices. *Nature* **2008**, 452, 732.
- (8) Ohtomo, A.; Hwang, H. Y. A high-mobility electron gas at the LaAlO₃/SrTiO₃ heterointerface. *Nature* **2004**, 427, 423.
- (9) Kim, U.; Park, C.; Ha, T.; Kim, Y. M.; Kim, N.; Ju, C.; Park, J.; Yu, J.; Kim, J. H.; Char, K. All-perovskite transparent high mobility field effect using epitaxial BaSnO₃ and LaInO₃ featured. *APL Mater.* **2015**, 3, 036101.
- (10) Liu, C.; Yan, X.; Jin, D.; Ma, Y.; Hsiao, H.-W.; Lin, Y.; Bretz-Sullivan, T. M.; Zhou, X.; Pearson, J.; Fisher, B.; Jiang, J. S.; Han, W.; Zuo, J.-M.; Wen, J.; Fong, D. D.; Sun, J.; Zhou, H.; Bhattacharya, A. Two-dimensional superconductivity and anisotropic transport at KTaO₃ (111) interfaces. *Science* **2021**, *371*, 716.
- (11) Xu, P.; Ayino, Y.; Cheng, C.; Pribiag, V. S.; Comes, R. B.; Sushko, P. V.; Chambers, S. A.; Jalan, B. Predictive control over charge density in the two-dimensional electron gas at the polar/non-polar NdTiO₃/SrTiO₃ interface. *Phys. Rev. Lett.* **2016**, *117*, 106803.
- (12) Ayino, Y.; Xu, P.; T-Lazo, J.; Yue, J.; Jalan, B.; Pribiag, V. Ferromagnetism and spin-dependent transport at a complex oxide interface. *Phys. Rev. Mater.* **2018**, *2*, 031401.
- (13) Lee, W.-J.; Kim, H. J.; Kang, J.; Jang, D. H.; Kim, T. H.; Lee, J. H.; Kim, K. H. Transparent Perovskite Barium Stannate with High Electron Mobility and Thermal Stability. *Annu. Rev. Mater. Res.* **2017**, 47, 301
- (14) Prakash, A.; Jalan, B. Wide Bandgap Perovskite Oxides with High Room-Temperature Electron Mobility. *Adv. Mater. Interfaces* **2019**, *6*, 1900479.
- (15) Prakash, A.; Xu, P.; Faghaninia, A.; Shukla, S.; Ager, J. W.; Lo, C. S.; Jalan, B. Wide bandgap BaSnO₃ films with room temperature conductivity exceeding 10⁴ S cm⁻¹. *Nat. Commun.* **2017**, 8 (1), 15167.
- (16) Paik, H.; Chen, Z.; Lochocki, E.; H, A. S.; Verma, A.; Tanen, N.; Park, J.; Uchida, M.; Shang, S.; Zhou, B.-C.; Brützam, M.; Uecker, R.; Liu, Z.-K.; Jena, D.; Shen, K. M.; Muller, D. A.; Schlom, D. G. Adsorption-Controlled Growth of La-doped BaSnO₃ by molecular-Beam Epitaxy. *APL Mater.* **2017**, *5* (11), 116107.
- (17) Cho, H. J.; Feng, B.; Onozato, T.; Wei, M.; Sanchela, A. V.; Ikuhara, Y.; Ohta, H. Investigation of electrical and thermal transport

- property reductions in La-doped BaSnO₃ films. *Physical Review Materials* **2019**, 3 (9), 094601.
- (18) Ganguly, K.; Prakash, A.; Jalan, B.; Leighton, C. Mobility-electron density relation probed via controlled oxygen vacancy doping in epitaxial BaSnO₃. *APL Mater.* **2017**, *5* (5), 056102.
- (19) Truttmann, T.; Prakash, A.; Yue, J.; Mates, T. E.; Jalan, B. Dopant solubility and charge compensation in La-doped SrSnO₃ films. *Appl. Phys. Lett.* **2019**, *115* (15), 152103.
- (20) Raghavan, S.; Schumann, T.; Kim, H.; Zhang, J. Y.; Cain, T. A.; Stemmer, S. High-mobility BaSnO₃ grown by oxide molecular beam epitaxy. *APL Mater.* **2016**, *4* (1), 016106.
- (21) Kim, H. J.; Kim, U.; Kim, T. H.; Kim, J.; Kim, H. M.; Jeon, B.-G.; Lee, W.-J.; Mun, H. S.; Hong, K. T.; Yu, J. Physical properties of transparent perovskite oxides (Ba,La)SnO₃ with high electrical mobility at room temperature. *Phys. Rev. B: Condens. Matter Mater. Phys.* **2012**, *86* (16), 165205.
- (22) Gao, Q.; Chen, H.; Li, K.; Liu, Q. Band Gap Engineering and Room-Temperature Ferromagnetism by Oxygen Vacancies in SrSnO₃ Epitaxial Films. *ACS Appl. Mater. Interfaces* **2018**, *10* (32), 27503–27509.
- (23) Gao, D.; Gao, X.; Wu, Y.; Zhang, T.; Yang, J.; Li, X. Co-doped $SrSnO_3$ epitaxial thin films on MgO with tunable band gap and room-temperature ferromagnetism. *Phys. E* **2019**, *109*, 101–106.
- (24) Wei, M.; Sanchela, A. V.; Feng, B.; Ikuhara, Y.; Cho, H. J.; Ohta, H. High electrical conducting deep-ultraviolet-transparent oxide semiconductor La-doped SrSnO₃ exceeding similar to 3000 Scm⁻¹. *Appl. Phys. Lett.* **2020**, *116*, 022103.
- (25) Yue, J.; Thoutam, L. R.; Prakash, A.; Wang, T.; Jalan, B. Unraveling the effect of electron-electron interaction on electronic transport in La-doped SrSnO₃ films. *Appl. Phys. Lett.* **2019**, *115* (8), 082102.
- (26) Chaganti, V. R. S. K.; Prakash, A.; Yue, J.; Jalan, B.; Koester, S. J. Demonstration of a Depletion-Mode SrSnO₃ n-Channel MESFET. *IEEE Electron Device Lett.* **2018**, 39 (9), 1381–1384.
- (27) Thoutam, L. R.; Yue, J.; Prakash, A.; Wang, T.; Elangovan, K. E.; Jalan, B. Electrostatic control of insulator—metal transition in Ladoped SrSnO₃ films. *ACS Appl. Mater. Interfaces* **2019**, *11*, 7666.
- (28) Chaganti, V. R. S. K.; Truttmann, T. K.; Liu, F.; Jalan, B.; Koester, S. J. SrSnO₃ field-effect transistors with recessed gate electrodes. *IEEE Electron Device Lett.* **2020**, *41*, 1428.
- (29) Wen, J.; Chaganti, V. R. S. K.; Truttmann, T. K.; Liu, F.; Jalan, B.; Koester, S. J. SrSnO₃ Metal-Semiconductor Field-Effect Transistor with GHz Operation. *IEEE Electron Device Lett.* **2021**, 42, 74.
- (30) Wang, T.; Prakash, A.; Dong, Y.; Truttmann, T.; Bucsek, A.; James, R.; Fong, D. D.; Kim, J.-W.; Ryan, P. J.; Zhou, H.; Birol, T.; Jalan, B. Engineering SrSnO₃ Phases and Electron Mobility at Room Temperature Using Epitaxial Strain. *ACS Appl. Mater. Interfaces* **2018**, 10 (50), 43802–43808.
- (31) Prakash, A.; Wang, T.; Bucsek, A.; Truttmann, T. K.; Fali, A.; Cotrufo, M.; Yun, H.; Kim, J.-W.; Ryan, P. J.; Mkhoyan, K. A.; Alu, A.; Abate, Y.; James, R. D.; Jalan, B. Self-Assembled Periodic Nanostructures Using Martensitic Phase Transformations. *Nano Lett.* 2021, 21, 1246.
- (32) Truttmann, T. K.; Liu, F.; Garcia-Barriocanal, J.; James, R. D.; Jalan, B. Strain Relaxation via Phase Transformation in SrSnO₃. ACS Appl. Electron. Mater. **2021**, *3*, 1127.
- (33) Lisunov, K. G.; Arushanov, E.; Thomas, G. A.; Bucher, E.; Schön, J. H. Variable-range hopping conductivity and magnetoresistance in n-CuGaSe₂. *J. Appl. Phys.* **2000**, *88* (7), 4128–4134.
- (34) Raikh, M. E.; Czingon, J.; Ye, Q.-y.; Koch, F.; Schoepe, W.; Ploog, K. Mechanisms of magnetoresistance in variable-range-hopping transport for two-dimensional electron systems. *Phys. Rev. B: Condens. Matter Mater. Phys.* **1992**, 45 (11), 6015–6022.
- (35) Raikh, M. E.; Wessels, G. F. Single-scattering-path approach to the negative magnetoresistance in the variable-range-hopping regime for two-dimensional electron systems. *Phys. Rev. B: Condens. Matter Mater. Phys.* **1993**, 47 (23), 15609–15621.
- (36) Wang, H.; Walter, J.; Ganguly, K.; Yu, B.; Yu, G.; Zhang, Z.; Zhou, H.; Fu, H.; Greven, M.; Leighton, C. Wide-voltage-window

Nano Letters pubs.acs.org/NanoLett Letter

- reversible control of electronic transport in electrolyte-gated epitaxial BaSnO₃. *Physical Review Materials* **2019**, 3 (7), 075001.
- (37) Wang, T.; Thoutam, L. R.; Prakash, A.; Nunn, W.; Haugstad, G.; Jalan, B. Defect-driven localization crossovers in MBE-grown Ladoped SrSnO₃ films. *Physical Review Materials* **2017**, *1* (6), 061601.
- (38) Shklovskii, B.; Efros, A. L. Electronic Properties of Doped Semiconductors; Springer: Berlin, 1984.
- (39) Faran, O.; Ovadyahu, Z. Magnetoconductance in the variable-range-hopping regime due to a quantum-interference mechanism. *Phys. Rev. B: Condens. Matter Mater. Phys.* **1988**, 38 (8), 5457–5465.
- (40) Ovadyahu, Z. Anisotropic magnetoresistance in a Fermi glass. Phys. Rev. B: Condens. Matter Mater. Phys. 1986, 33 (9), 6552-6554.
- (41) Fischbach, J. U.; Rühle, W.; Bimberg, D.; Bauser, E. Experimental determination of the anisotropy of the exciton wave function of GaAs in a magnetic field. *Solid State Commun.* 1976, 18 (9), 1255–1258.
- (42) Ye, Q.-y.; Shklovskii, B. I.; Zrenner, A.; Koch, F.; Ploog, K. Hopping Transport in δ doping layers in GaAs. *Phys. Rev. B: Condens. Matter Mater. Phys.* **1990**, *41*, 8477.
- (43) Ke, X.; Adamo, C.; Schlom, D. G.; Bernhagen, M.; Uecker, R.; Schiffer, P. Low temperature magnetism in the perovskite substrate DyScO₃. Appl. Phys. Lett. **2009**, 94 (15), 152503.
- (44) Raekers, M.; Kuepper, K.; Bartkowski, S.; Prinz, M.; Postnikov, A. V.; Potzger, K.; Zhou, S.; Arulraj, A.; Stüßer, N.; Uecker, R.; Yang, W. L.; Neumann, M. Electronic and magnetic structure of RScO₃ (R = Sm, Gd, Dy)from x-ray spectroscopies and first-principles calculations. *Phys. Rev. B: Condens. Matter Mater. Phys.* **2009**, 79 (12), 125114.
- (45) Wu, Y.-D.; Chen, H.; Hua, J.-Y.; Qin, Y.-L.; Ma, X.-H.; Wei, Y.-Y.; Zi, Z.-F. Giant reversible magnetocaloric effect in orthorhombic GdScO₃. *Ceram. Int.* **2019**, 45 (10), 13094–13098.
- (46) Kamba, S.; Goian, V.; Nuzhnyy, D.; Bovtun, V.; Kempa, M.; Prokleška, J.; Bernhagen, M.; Uecker, R.; Schlom, D. G. Polar phonon anomalies in single-crystalline TbScO₃. *Phase Transitions* **2013**, *86*, 206
- (47) Wu, Y.-D.; Qin, Y.-L.; Ma, X.-H.; Li, R.-W.; Wei, Y.-Y.; Zi, Z.-F. Large rotating magnetocaloric effect at low magnetic fields in the Ising-like antiferromagnet DyScO₃ single crystal. *J. Alloys Compd.* **2019**, 777, 673.